Journal of Engineering Science and Technology Review 17 (5) (2024) 94-103

Research Article

JOURNAL OF
Engineering Science and Technology Review

www.jestr.org

Numerical Simulation on Diffusion Behavior of Corrosion Ion in Concrete under Fatigue

Wenzheng He[1,*] and Jing He[2]

[1]*School of Urban Construction Engineering, Chongqing Open University, Chongqing 401520, China*
[2]*Department of Mathematics and Science, Chongqing College of Mobile Communication, Chongqing 401520, China*

Received 9 August 2024; Accepted 17 October 2024

Abstract

In corrosive environments, concrete structures, such as roads and tunnel inverts, are adversely affected by the combined effects of corrosion and fatigue loading. Fatigue loading accelerates the transmission of corrosion ions, resulting in a rapid degradation of structural performance. To examine the transmission law of corrosion ions under fatigue load, this study proposed an unsteady transmission model of corrosion ions in concrete. In view of the interaction between composite corrosion ions, a set of sulfate–chloride ion coupling transmission equations was established based on Fick's second law. Subsequently, fatigue load parameters were introduced into the corrosion ion diffusion coefficient function according to the concrete fatigue equation, and a corrosion ion transport model under fatigue load was established. Moreover, the influence of fatigue parameters on ion transport behavior was discussed based on parameter analysis. Results demonstrate that fatigue load can accelerate the transmission of corrosion ions, and the corrosion rate is positively related to loading frequency and stress level. However, when the stress level is less than 0.2, fatigue load has little effect on the transmission rate of corrosion ions. This study establishes a link between fatigue load and corrosion ion transport behavior and provides a method for assessing the durability of concrete in corrosive environments.

Keywords: Concrete, Fatigue load, Corrosive ion, Diffusion

1. Introduction

Rock formations containing corrosive minerals are widely distributed in southwestern China. The groundwater in these areas contains high concentrations of sulfate and chloride ions, exposing concrete structures such as roads, tunnels, and bridges to sulfate–chloride compound corrosion environment [1]. At present, high-speed passenger transportation and heavy-duty freight transportation have become inevitable trends. Roads and bridges bear large vibration loads because of large axle load and high-density operation of vehicles. In the aforementioned formations rich in corrosive salts, the coupling effect of vibration load and corrosion can accelerate structural damage. Corrosion cracking of some concrete structures in these areas has already become a serious problem.

The corrosion process of concrete is complex, involving the coupling of multiple factors, including the diffusion of corrosive ions within the material and damage under static and impact fatigue loads. In addition, various environmental factors further complicate the corrosion process. Therefore, the corrosion process of concrete involves numerous factors, and the high degree of coupling between these factors presents significant challenges for studying the fatigue damage of concrete structures in corrosive environments.

Numerous studies have been conducted on the corrosion of concrete structures [2-3]. However, the corrosion ion transport model under fatigue loading still requires further investigation. An urgent problem to solve is how to reasonably introduce fatigue load into the concrete corrosion equation and clarify the coupling relationship between corrosion and fatigue.

Based on the above analysis, this study used mathematical mechanical methods to establish a set of corrosion ion diffusion–reaction differential equations under fatigue load to examine the concentration distribution characteristics of chloride and sulfate ions in concrete. Moreover, the study analyzed the influence of fatigue load on corrosion ion transmission behavior. The aim is to accurately simulate the concrete corrosion process under fatigue load, thereby providing a reference for evaluating the durability of concrete structures in saline environments.

2. State of the art

At present, numerous studies have been conducted on the corrosion of concrete, focusing primarily on experimental and theoretical models. In experimental studies, scholars have explored the mechanical properties, physical parameters, and microstructure of concrete under corrosive conditions. Fernando Silva et al. [4] assessed the compressive strength of self-compacting concrete under sulfate attack. Uwanyuze et al. [5] used electron backscatter diffraction and energy dispersive X-ray spectroscopy to study the degradation of concrete attacked by sulfate. Their study achieved a precise correlation between elemental composition and mineral crystal phase diagrams. Cefis et al. [6] conducted an experimental study to evaluate the effect of external sulfate attack on structural concrete. Over a three-year period, they monitored the overall expansion of specimens caused by chemical reactions and measured the increase in surface porosity due to sulfate attack. Tanyildizi [7] examined the mechanical properties and microstructure

*E-mail address: hewenzheng1982@126.com
ISSN: 1791-2377
doi:10.25103/jestr.175.13

of polymer mortar after sulfate attack but did not measure the microscopic distribution of corrosive ions.

The aforementioned experimental studies did not consider the influence of chloride ions, focusing solely on the performance of concrete under sulfate corrosion. However, some scholars have conducted experiments on the problem of chloride–sulfate composite corrosion and have obtained valuable results. Soleimanirad et al. [8] examined the effect of chloride ions on the corrosion resistance of concrete under sulfate erosion. They found that although the chloride ions reduced the degree of concrete deterioration under sulfuric acid attack, it increased the probability of steel bars rusting in a sulfate environment. Nie et al. [9] explored the dynamic response of concrete under the combined influence of chloride and sulfate ions. They established the stress–strain relationship of concrete in sodium chloride and sodium sulfate solutions. Rusati et al. [10] conducted experimental studies on the macroscopic properties of cement inorganic binder mixtures exposed to magnesium chloride and magnesium sulfate. However, they did not study the transport characteristics of microscopic ions under the combined corrosion of chloride and sulfate salts.

In terms of theoretical study, most of the existing studies have focused on corrosion ion transport equations and the simulation of damage resulting from corrosion. Islam et al. [11] developed a chemical mechanics model for cement-stabilized pavement bases, establishing corresponding control equations and determining the relationship between the sulfate diffusion coefficient, temperature, and humidity. This model accurately describes the damage process of cement-stabilized pavement bases due to sulfate corrosion, but it only considers sulfate corrosion, neglecting chlorine salt corrosion. Chen et al. [12] proposed a multiphase mesoscopic numerical model for sulfate corrosion. This model incorporated a dissolution equilibrium equation to simulate the leaching of solid-phase calcium and the dissolution of solid-phase aluminate, demonstrating that ignoring solid-phase calcium leaching underestimates the sulfate attack capability. Zuo et al. [13] established a microscopic model to depict the deterioration of cement-based materials under sulfate attack, geometrically reconstructing the components in concrete to reflect their heterogeneity. Yin et al. [14] developed a comprehensive macro–micro model for concrete deterioration under sulfate attack. The model introduced a critical parameter related to crystallization pressure, which establishes criteria for the boundary movement of concrete specimens caused by sulfate attack. He et al. [15] used mathematical and mechanical methods to establish a system of sulfate–chloride ion coupling diffusion equations and derived an evolution model for the bearing capacity of reinforced concrete linings under sulfate corrosion. This model can simulate the entire micro-macro damage process of lining corrosion deterioration. Guan et al. [16-17] investigated the transmission mechanism of chloride ions in concrete under alternating load and established an ion transport model for chlorine damage in concrete based on Fick's second law. Although this model can assess the influence of fatigue load on ion transport behavior, it simplifies the diffusion coefficient by not considering its time-varying characteristics and is limited to calculating the transmission behavior of a single chloride ion without considering the combined effects of chloride and sulfate ions.

The aforementioned studies focused on sulfate or chloride corrosion processes. However, theoretical and experimental investigations into the effects of fatigue load, especially the combined effects of fatigue load and composite corrosion, are scarce. This study explored the corrosion behavior of concrete under fatigue load. Based on the diffusion reaction theory, a system of sulfate–chloride ion coupling transmission equations was established considering the interaction between composite corrosion ions. Fatigue load parameters were introduced into the corrosion ion diffusion coefficient function, resulting in the development of a corrosive ion transmission model under fatigue load. Through parameter analysis, the influence of fatigue parameters on ion transmission behavior was explored. This study introduced a method to assess the durability of concrete structures subjected to fatigue loads in corrosive environments.

The remainder of this study is structured as follows. Section 3 constructs an ion migration model under the combined effects of fatigue load and corrosion. In Section 4, numerical analysis is used to determine the ion concentration distribution law influenced by fatigue load. Finally, Section 5 summarizes the study and presents the relevant conclusions.

3. Methodology

3.1 Corrosion ion transport equation

Regarding the problem of concrete being co-corroded by chloride salt and sulfate, the academic consensus is that chloride salt and sulfate inhibit each other during the diffusion process in concrete. However, this study challenges that notion, arguing it is not completely accurate. As sulfate ions diffuse further, the corrosion causes expansion and cracking within the concrete, thereby accelerating the transmission of chloride ions. During the coupling transmission process of sulfate–chloride ions, the transmission rate of ions is constantly evolving, and there remains a lack of accurate theoretical study on this process. This section initially establishes the coupling transmission equation for chloride and sulfate ions. On this basis, fatigue load parameters are introduced to adjust the diffusion coefficient. Finally, an ion migration model under fatigue–corrosion coupling is established.

3.1.1 Chloride–sulfate ion coupling transport equation

Chloride ions in concrete exist in two forms, namely, free and combined chloride ions, of which free chloride ions are responsible for the corrosion of steel reinforcement in concrete [18]. The equation for free chlorine ions transport is as follows:

$$\begin{cases} \dfrac{\partial C}{\partial t} = \dfrac{\partial}{\partial x}\left[\dfrac{D_C(x,t)}{1+J}\dfrac{\partial C}{\partial x}\right] \\ C(x,0) = C_0, C(0,t) = C_s(t), x \in (0,\ l) \end{cases} \tag{1}$$

where C is the free chloride ion concentration, C_0 is the initial chloride ion concentration (initial condition), J is the reaction equilibrium constant, $D_C(x,t)$ is the diffusion coefficient function, $C_s(t)$ is the time-varying function of chloride ion concentration on the concrete surface (boundary condition), x is the cross-sectional position, t is the corrosion time, and l is the section width.

According to the method in [19], in a compound corrosion environment, the effect of sulfate corrosion product packing on chloride ion diffusion capacity can be simulated by correcting its diffusion coefficient, which can be expressed as:

$$D_C(x,t) = D_C^{'}\left(1 - k_{ts}U_D\right) \tag{2}$$

where $D_C(x,t)$ is the chloride ion diffusion coefficient after considering the filling effect of sulfate corrosion products, $D_C^{'}$ is the chloride ion diffusion coefficient without considering the filling effect, k_{ts} is the filling influence coefficient of sulfate corrosion products, and U_D is the amount of sulfate ions consumed by the reaction.

Similarly, the effect of chloride ions on sulfate ion transport capacity can be characterized by the following formula:

$$D_{SO_4^{2-}}(x,t) = D_{SO_4^{2-}}^{'}\left(1 - k_{tc}C\right) \tag{3}$$

where $D_{SO_4^{2-}}(x,t)$ is the sulfate ion diffusion coefficient considering the influence of chloride ions; $D_{SO_4^{2-}}^{'}$ is the sulfate ion diffusion coefficient without considering the influence of chloride ions; k_{tc} is the chloride ion influence coefficient, which is used to characterize the influence of Friedel salt produced by chloride ions on the diffusion performance of sulfate ions; and C denotes the chloride ion concentration.

Combined with the sulfate diffusion–reaction theory, the sulfate ion diffusion–reaction equation considering the influence of chloride ions can be modified as follows:

$$\begin{cases} \dfrac{\partial U_{SO_4^{2-}}}{\partial t} = \dfrac{\partial}{\partial x}\left[D_{SO_4^{2-}}^{'}\left(1 - k_{tc}C\right)\dfrac{\partial U_{SO_4^{2-}}}{\partial x} \right] - \dfrac{\partial U_D}{\partial t} \\ U_{SO_4^{2-}}(x,0) = U_0, U_{SO_4^{2-}}(0,t) = U_s(t), x \in (0,\ l) \end{cases} \tag{4}$$

where U_0 is the initial sulfate ion concentration, and $U_s(t)$ is the sulfate ion concentration on the concrete surface.

In addition, during the diffusion process, sulfate ions react with calcium hydroxide to generate secondary gypsum. The consumption of sulfate ions during this reaction can be expressed as follows:

$$\begin{cases} \dfrac{\partial U_D}{\partial t} = k_1 U_{SO_4^{2-}} U_{ca^{2+}} \\ U_D(x,0) = 0 \end{cases} \tag{5}$$

where k_1 is the reaction rate constant to generate secondary gypsum, and $U_{ca^{2+}}$ is the calcium ion concentration in the pore solution.

CA is a collection of aluminum-containing phase compounds in concrete. The reaction rate equation for reacting with the secondary gypsum to form ettringite is as follows:

$$\begin{cases} \dfrac{\partial U_{CA}}{\partial t} = -\dfrac{k_2 U_{SO_4^{2-}} U_{CA}}{q} \\ U_{CA}(x,0) = U_{CA0} \end{cases} \tag{6}$$

where U_{CA} is the CA concentration in concrete, U_{CA0} is the initial CA concentration in concrete, k_2 is the reaction rate constant that CA reacts with the secondary gypsum to form ettringite, and q is the weighted average coefficient. The consumption of CA during the reaction can be expressed as follows:

$$U_{RCA} = U_{CA0} - U_{CA} \tag{7}$$

where U_{CA0} is the initial CA concentration.

The time-varying model of surface corrosion ion concentration under sulfate–chlorate joint corrosion is still described by an exponential model [15]. In view of the influence of sulfate, the time-varying model of surface chloride ion concentration is as follows:

$$C_s(t) = C_0 + \left[g_1(w/c) + c_1 \right]\left(d_1 m_{su} + j_1\right) C_{\max}\left(1 - e^{-ht}\right) \tag{8}$$

Similarly, the time-varying function of surface sulfate ion concentration considering the influence of chlorine salt is as follows:

$$U_s(t) = U_0 + \left[g_2(w/c) + c_2 \right]\left(d_2 m_{sc} + j_2\right) U_{\max}\left(1 - e^{-gt}\right) \tag{9}$$

where C_0 and U_0 are the initial concentrations of chloride and sulfate ions, respectively; $C_{\max}$ and $U_{\max}$ are the increment of the surface chloride ion and sulfate ion concentrations after stabilization, respectively; m_{sc} is the concentration of chloride salt in the composite solution; m_{su} is the sulfate concentration in the composite solution; w/c is the water–cement ratio; and g, c, d, and j are fitting parameters, which can be fitted through experimental values.

By combining Eqs. (1), (4), (5), and (6), a set of sulfate–chloride ion coupling diffusion equations can be obtained.

3.1.2 Equivalent macroscopic expansion strain

The ettringite generated by the reaction initially fills the pores. After the pores are filled to the maximum, the ettringite that continues growing will squeeze the pore walls and produce expansion strain. In view of the filling effect of the ettringite, the expansion volume of concrete caused by corrosion is as follows:

$$\varepsilon_{vs} = Max\left(\varepsilon_{vt} - f\varphi_0, 0\right) \tag{10}$$

where f is the effective filling coefficient, with a value of 0.3–0.4, ε_{vt} is the unit volume change of concrete caused by chemical reaction, and φ_0 is the initial porosity.

According to elastic mechanics, volume strain is converted into linear strain:

$$\varepsilon_R^P = \frac{\varepsilon_{vs}}{3} \tag{11}$$

where ε_R^P is the free expansion linear strain of the ettringite obtained based on the microscopic volume expansion process. The deterioration damage of concrete cannot be measured from a macro perspective, which should be converted into equivalent macro strain. Taking a sphere with unit volume in concrete, the effective elastic modulus and shear modulus of the unit sphere are as follows:

$$\begin{cases} k^p = k_{ett}\left(1-\dfrac{3\varphi^m f_w k_{ett}+4\varphi^m f_w \mu_{ett}}{3\varphi^m f_w k_{ett}+4\mu_{ett}}\right) \\ \mu^p = \mu_{ett}\left[1-\left(\varphi^m f_w\right)^2\right] \end{cases} \tag{12}$$

where φ^m is the volume unit for porosity, k_{ett} is the bulk modulus of ettringite, μ_{ett} is the shear modulus of ettringite; and f_w is the percentage of pore space occupied by the solution in the pores, which can be expressed as follows:

$$f_w=\frac{4\mu_{ett}\left(k_{ett}-k_w\right)}{k_{ett}\left(3k_{ett}+4\mu_{ett}\right)} \tag{13}$$

where k_w is the bulk modulus of the pore solution.

The equivalent macroscopic line strain of concrete caused by the growth of ettringite is as follows:

$$\varepsilon_{ett}=\frac{9\varphi^m k^p}{3k^p+4\mu^s}\varepsilon_R^P \tag{14}$$

where μ^s is the shear modulus of the concrete matrix.

3.1.3 Influence of static load

A static load not only changes the porosity of concrete but also aggravates or inhibits the formation and growth of cracks within the concrete. This is particularly evident at high load levels when concrete transitions into a plastic state and may even fail, resulting in numerous cracks, including visible macroscopic ones. The effect of loading on porosity and dilatational strain will be derived as follows.

Jin et al. [20] studied the variation law of concrete porosity under load, and according to their theory, the porosity of concrete under load can be expressed as follows:

$$\varphi_L=\frac{\varphi_0}{1-\varepsilon_{ve}}\left[1-\frac{\left(4G_m+3K_m\right)\Theta}{4G_m+3K_m\varphi_0}\right]^3 \tag{15}$$

where ε_{ve} is the volumetric strain generated by the load, K_m is the bulk modulus of concrete, μ is the Poisson's ratio of concrete, G_m is the shear modulus of concrete, and $\Theta=1-\sqrt[3]{1-\varepsilon_{ve}}$.

The linear strains produced by axial loads are converted into volumetric strains:

$$\varepsilon_{ve}=\left(1-2\mu\right)\varepsilon_{le} \tag{16}$$

where ε_{le} is the linear strain generated by the axial load.

When concrete suffers from sulphate attack, the ettringite will initially fill the capillary pores of the concrete. In view of the filling effect, the change in capillary porosity can be expressed as follows:

$$\Delta\varphi = Min\left(\varepsilon_{vt}, f\varphi_0\right) \tag{17}$$

In view of the axial load and filling effect of corrosion products, the concrete porosity can be expressed as follows:

$$\varphi=\varphi_L-\Delta\varphi \tag{18}$$

The equivalent line strain under the combined action of axial load and corrosion is:

$$\varepsilon=\varepsilon_{ett}+\varepsilon_{le} \tag{19}$$

However, under normal circumstances, the volumetric strain in concrete due to external static load is minimal, resulting in only a slight change in void ratio. The primary influence of static load on ion transmission is through its effect on cracks.

3.1.4 Diffusion coefficient model

The diffusion coefficients $D(x,t)$ of chloride and sulfate ions are binary functions of time t and position x, which characterize the ion transmission capacity of concrete at different times and positions, respectively. The influencing factors of the diffusion coefficient can be summarized as follows: Prior to concrete cracking, porosity plays a controlling role in diffusion coefficient. After cracking, the cracks play a controlling role in the diffusion coefficient.

Before corrosion expansion cracking occurs in concrete, the diffusion coefficient is a function of porosity. The initial diffusion coefficient of corrosion ions in concrete is as follows:

$$\begin{aligned} D_0=&\Gamma\left(\varphi_0\right)=D^\mu\left[0.001+0.07\varphi_0^2+\right. \\ &\left.H\left(\varphi_0-0.18\right)\times 1.8\times\left(\varphi_0-0.18\right)^2\right] \end{aligned} \tag{20}$$

where D^μ is the diffusion coefficient of corrosion ions in the solution, φ_0 is the initial porosity, and $H(x)=\begin{cases}1 & x>0\\ 0 & x\le 0\end{cases}$.

When the pores of concrete are filled with ettringite, the void ratio and the diffusion coefficient decrease. The method in [21] can be used to calculate the diffusion coefficient, considering the filling effect:

$$D_s=D_{\min}+\left(D_0-D_{\min}\right)\frac{e^{-\beta_D}\dfrac{\varphi}{\varphi_0}}{1+\left(e^{-\beta_D}-1\right)\dfrac{\varphi}{\varphi_0}} \tag{21}$$

where β_D is the shape coefficient, and $D_{\min}=0.1D_0$.

Crack density function d_{cr} is used to characterize the evolution characteristics of concrete microcracks, and it can be expressed as follows:

$$d_{cr}=\begin{cases}0 & \varepsilon \le \varepsilon_{th} \\ \chi\left(1-\dfrac{\varepsilon_{th}}{\varepsilon}\right)^{\kappa} & \varepsilon > \varepsilon_{th}\end{cases} \tag{22}$$

where χ and κ are the parameters related to the concrete strength grade, and ε_{th} is the critical strain.

The diffusion coefficient after the crack appears is as follows:

$$D_{crack}=D_0\left[\left(1+\frac{32}{9}d_{cr}\right)+D_P\right] \tag{23}$$

$$D_P=\begin{cases}0 & d_{cr}<C_{dc} \\ \dfrac{\left(d_{cr}-C_{dc}\right)^2}{C_{dec}-d_{cr}} & C_{dc}<d_{cr}<C_{dec}\end{cases} \tag{24}$$

where C_{dc} is the crack density corresponding to ε_p (strain corresponding to peak stress), with a value of 0.182, and C_{dec} is the crack density corresponding to limit tensile strain, with a value of 0.712.

The entire process expression of the diffusion coefficient can be summarized as follows:

$$D(x,t)=\begin{cases}D_s & \varepsilon \le \varepsilon_{th} \\ D_0\left(1+\dfrac{32}{9}d_{cr}\right) & \varepsilon_{th}<\varepsilon \le \varepsilon_p \\ D_0\left[\left(1+\dfrac{32}{9}d_{cr}\right)+\dfrac{\left(d_{cr}-C_{dc}\right)^2}{C_{dec}-d_{cr}}\right] & \varepsilon_p<\varepsilon \le \varepsilon_u \\ D_{\max} & \varepsilon_u<\varepsilon\end{cases} \tag{25}$$

where $D_{\max}$ is the ion diffusion coefficient when the expansion strain exceeds ε_u, and $D_{\max}$ takes 10 times the initial diffusion coefficient.

According to Eq. (25), the corrosion ion diffusion coefficient under the influence of environmental factors, such as load, can be calculated.

3.2 Fatigue correction of diffusion coefficient

3.2.1 Characterization of corrosion ion diffusion coefficient based on crack factor

Concrete components subjected to fatigue loads can be divided into two parts based on the different diffusion pathways of corrosion ions: new cracks and the matrix. The transmission of corrosion ions under fatigue load can be equivalent to the diffusion of ions in new cracks and the concrete matrix [16-17]. The total diffusion quantity is the sum of the corrosion ions diffused through the two pathways. Assuming homogeneous diffusion of corrosion ions within the matrix material, the cracks generated by bending fatigue load quickly become filled with the salt solution; thus, the diffusion of corrosion ions in new cracks can be regarded as diffusion in the solution. Therefore, the transmission of corrosion ions under fatigue load can be regarded as the sum of their migration in the concrete matrix and in the solution.

When a concrete member is subjected to fatigue bending load, new micro cracks are generated during the loading process and existing cracks expand. A vacuum state forms at the crack tip, causing corrosive ions to be rapidly drawn into the concrete interior due to the "pumping effect." During the unloading process, some corrosion ions return to the solution because the cracks close. This alternating loading and unloading process facilitates the diffusion of corrosion ions around microcracks, creating a "turbulence effect" that accelerates their diffusion.

The direction of crack expansion under bending load is assumed to be consistent with the migration direction of corrosion ions and perpendicular to the eroded bending surface. Assume that H_c is the diameter of new cracks; and H_m is the spacing between concrete matrix, including the diameter of new cracks. The relationship of the effective diffusion coefficient D_t, the diffusion coefficient in cracks D_c, and the diffusion coefficient in matrix concrete D_m can be expressed as follows [17]:

$$\frac{D_t}{D_m}=1+0.785\varepsilon_1\times\frac{D_c}{D_m}-0.785\varepsilon_1 \tag{26}$$

where $\varepsilon_1=\dfrac{H_c}{H_m}$.

According to Eq. (26), the amplification factor of fatigue load on the ion diffusion coefficient in concrete can be calculated.

3.2.2 Parameter of fatigue load action

Fatigue load causes concrete damage, and concrete fatigue damage can be characterized by residual strain. The residual strain is caused by plastic deformation and cracks, and it can be equivalent to the maximum width of transverse microcracks generated under fatigue load [17], that is, $\xi_1=2L_{cone}$. Cracks are uniformized into cylindrical shape cracks, and $L_{cone}=\xi_1/2$. L is the initial length of the selected element. The relationship between the crack factor and residual deformation under alternating load can be expressed as follows:

$$\varepsilon_1=\frac{H_c}{H_m}=\frac{\dfrac{\xi_1}{2}}{L+\dfrac{\xi_1}{2}}=\frac{\xi_1/L}{2+\xi_1/L} \tag{27}$$

ξ_1/L is exactly the residual deformation of the concrete specimen after loading n times of fatigue load, that is, $\varepsilon_n^p=\xi_1/L$, which is substituted into Eq. (27):

$$\varepsilon_1=\frac{1}{\dfrac{2}{\varepsilon_n^p}+1} \tag{28}$$

ε_n^p can also be expressed as follows:

$$\varepsilon_n^p=F(T,n) \tag{29}$$

According to the linear fatigue cumulative damage theory of concrete, the relationship between the damage variable *d* and the number of loading cycles *n* is as follows:

$$d=\frac{n}{N_f} \tag{30}$$

where N_f is the concrete fatigue life.

The number *n* of fatigue loading can be expressed by the loading frequency *f* and the loading time *t*, with the following relationship:

$$n=ft \tag{31}$$

According to the linear fatigue cumulative damage theory, the concrete fatigue equation can be expressed as follows:

$$S=a-b\cdot\lg N_f \tag{32}$$

where *S* is the stress level, and *a* and *b* are experimental constants.

According to the fatigue damage mechanism of concrete materials, the damage to concrete components subjected to bending loads can be divided into three stages. In the first and second stages, the residual tensile strain shows a linear growth trend. Therefore, the development of residual tensile strain is consistent with changes in the relative cycle life ratio. For simplicity in calculation, the residual deformation during the first two stages of concrete fatigue damage is assumed to change linearly, accounting for approximately 90% of the concrete's entire fatigue load service life. By using the cycle ratio equivalence relationship, the following equation can be obtained:

$$\frac{n}{0.9N_f}=\frac{\varepsilon_n^p}{\varepsilon_B^p} \tag{33}$$

where ε_B^p is the corresponding residual strain at the end of the second development stage in the concrete fatigue damage process.

From Eqs. (32) and (33), the following equation can be obtained:

$$\frac{ft}{0.9\times10^{(a-S)/b}}=\frac{\varepsilon_n^p}{\varepsilon_B^p} \tag{34}$$

Therefore, the residual deformation after applying *n* fatigue loads is as follows:

$$\varepsilon_n^p=\frac{ft\times\varepsilon_B^p}{0.9\times10^{(a-S)/b}} \tag{35}$$

By substituting Eqs. (28) and (35) into Eq. (26), the corrected diffusion coefficient accounting for fatigue load can be obtained:

$$D_t=D_m+0.785\times\frac{ft\times\varepsilon_B^p\times D_m}{2\times0.9\times10^{(a-S)/b}+ft\times\varepsilon_B^p}\times\left(\frac{D_c}{D_m}-1\right) \tag{36}$$

where D_m can be calculated according to Eq. (25).

Given the presence of fatigue bending load, the solution near the new cracks flows due to the crack opening and closing caused by the loading and unloading process, resulting in a rapid increase in the migration rate of corrosion ions. When the solution flows, the diffusion coefficient of corrosion ions in the cracks D_c can be taken as 50 times D_0, and the corresponding residual strain ε_B^p at the end of the second development stage in the concrete fatigue damage process can be taken as 1.2×10^{-4}.

4. Result Analysis and Discussion

By combining Eqs. (1), (4), (5), and (6), the system of controlling partial differential equations can be obtained, and the diffusion coefficient function is calculated according to Eq. (36). This is a strongly coupled nonlinear system of equations, for which analytical solutions cannot be obtained. Therefore, this study used Comsol Multiphysics software to solve this system of equations through numerical analysis methods.

4.1 Calculation parameters

According to the unsteady corrosion ion transport model proposed in this study, the corrosion ion diffusion behavior in the specimen was calculated. A concrete specimen with a thickness of 0.1 m was taken as the study object, as shown in Fig. 1. The values of main parameters are shown in Table 1.

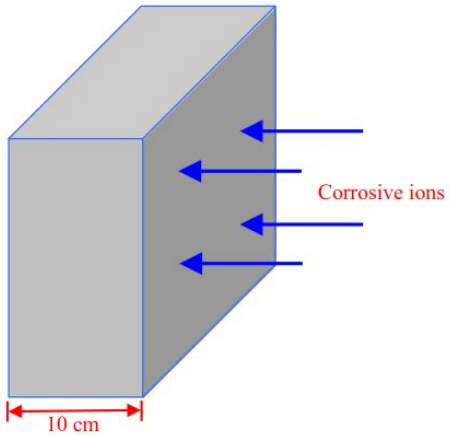

Fig. 1. One-dimensional corrosion

Table 1. Main parameters in the model

Parameters	Unit	Value
U_{max}	mol/m^3	330
C_{max}	mol/m^3	120
L	m	0.1
χ	—	1.77
κ	—	5.61
k_1	s^{-1}	1.22×10^{-8}
k_2	s^{-1}	1.22×10^{-9}
w/c	—	0.57
a	—	1.07
b	—	0.09

4.2 Calculation results

After solving the equation set, the data were organized to reveal the distribution patterns of sulfate ion and chloride ion

concentrations, as shown in Figs. 2-5. Fig. 2 displays the curve of sulfate ion concentration at a specific moment, and Fig. 3 presents the time-varying behavior of sulfate ion concentration at depths of 1, 10, and 20 mm. The calculation results indicate that the sulfate ion content within the concrete is negatively correlated with depth. At any given time, the ion concentration decreases as depth increases. However, the time-varying patterns of sulfate ion concentration differ depending on the location. For instance, the sulfate ion content on the concrete surface (x=1 mm) consistently increases over time. By contrast, the ion concentration within the concrete (x=10 mm and x=20 mm) initially increases and then decreases. This behavior can be explained by the chemical reactions during the early stages of corrosion, which consume sulfate ions at a low rate (the reaction rate is related to the concentration of free sulfate and calcium ions). During this stage, the rate of ion accumulation and replenishment via diffusion exceeds the ion consumption rate, leading to an upward trend in free sulfate ion concentration. However, in the later stages of corrosion, the reaction rate increases, causing the rate of ion replenishment and accumulation via diffusion to fall below the ion consumption rate, resulting in a decline in sulfate ion concentration.

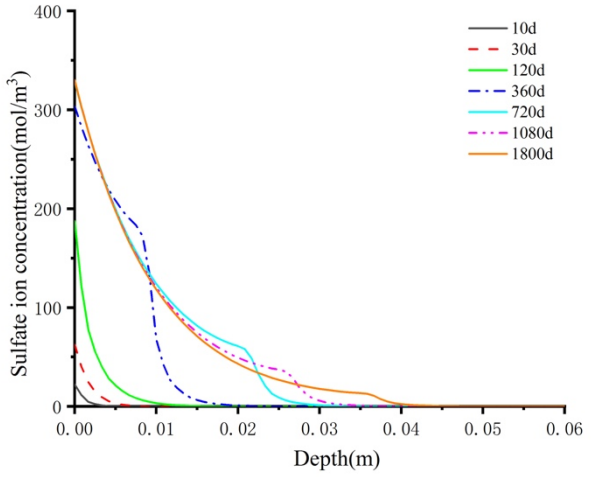

Fig. 2. Sulfate ion concentration curve at a typical time

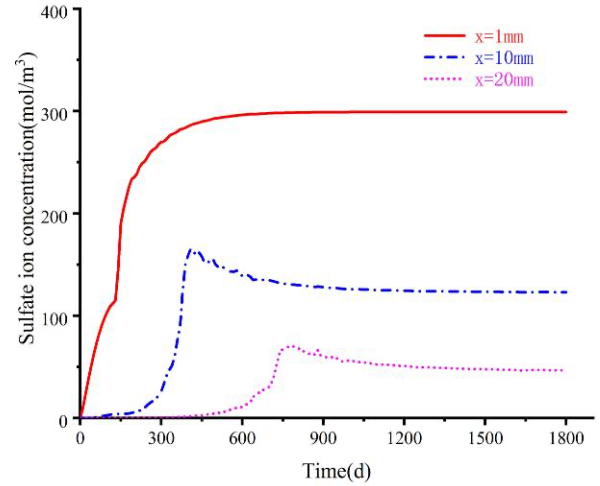

Fig. 3. Time-varying curve of sulfate ion at different depths

Fig. 4 shows the concentration distribution curve of chloride ions at various typical moments, and Fig. 5 shows the curves of chloride ion concentration at 1, 10, and 20 mm inside the concrete. The chloride ion concentration at each depth within the concrete increases monotonically with time until it reaches a stable value, which is greatly different from the sulfate ion transmission characteristics. Chloride ions are consumed because they do not chemically react with cement components. Overall, the transmission rate of chloride ion is considerably higher than that of sulfate ions, and on day 1800, chloride ions penetrate through the specimen.

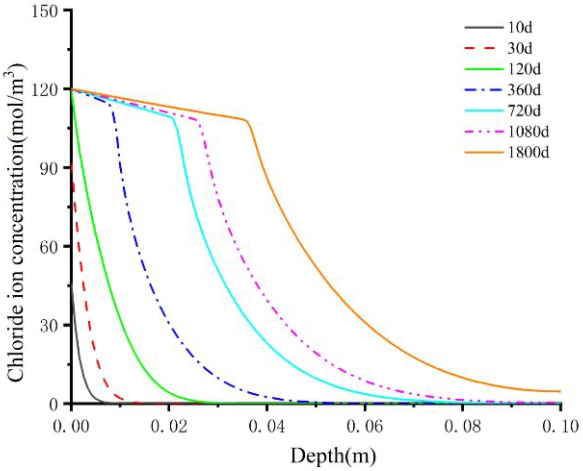

Fig. 4. Chloride ion concentration curve at a typical time

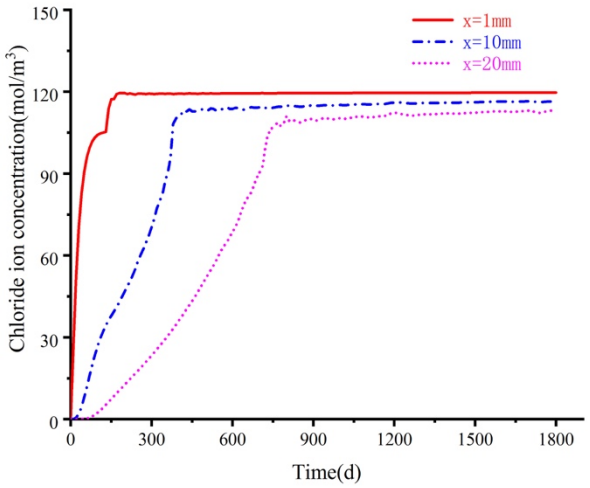

Fig. 5. Time-varying curve of chloride ion at different depths

To analyze the mutual influence between sulfate and chloride ions when both are present, this paper considers four operating conditions: (1) single salt solutions of Na_2SO_4 and $NaCl$; and (2) composite solutions of Na_2SO_4 and $NaCl$, particularly Na_2SO_4 ($NaCl$) with 2%, 5%, and 10% of $NaCl$ (Na_2SO_4).

Fig. 6 shows the time-varying curve of sulfate ion concentration at a depth of 10 mm under different concentrations of chloride ions. The distribution pattern of sulfate ion content in concrete remains consistent across various chloride salt concentrations. Theoretically, this suggests that although the presence of chloride salts does not change the corrosion mechanism of sulfates, it reduces the transmission rate of sulfate ions. Higher chloride concentrations correspond to lower sulfate ion content because the Friedel salt formed from the reaction between chloride ions and cement hydration products fills some of the concrete's pores. This filling reduces the porosity and thus delays the transmission of sulfate ions. As chloride concentration increases, more Friedel salts are produced,

enhancing the inhibitory effect. Therefore, chloride ions inhibit the diffusion of sulfate ions throughout the entire corrosion period.

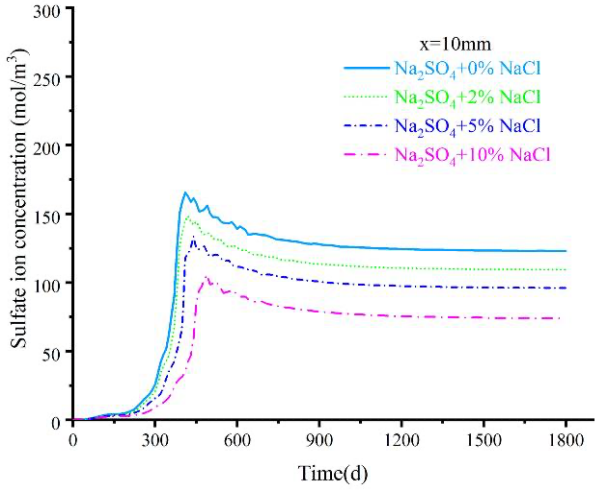

Fig. 6. Effect of chloride ions on sulfate ion transmission

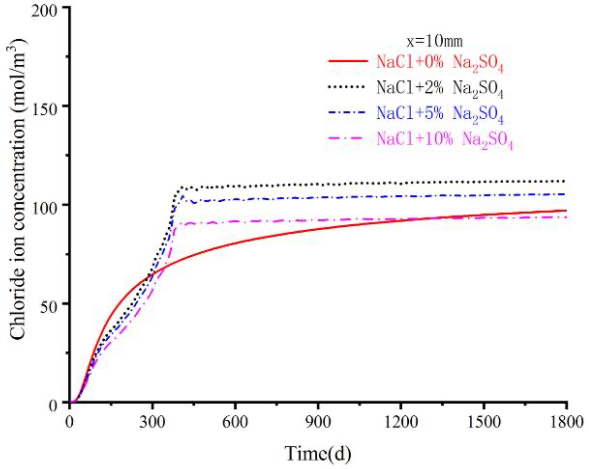

Fig. 7. Effect of sulfate on chloride ion transmission

Fig. 7 shows the time-varying curve of chloride ion concentration at a depth of 10 mm under the influence of different concentrations of sulfate ions. The calculation results indicate that the evolution of chloride ions influenced by sulfate can be divided into two stages. During the first stage (before corrosion cracking), the concrete has not cracked yet because the expansion of sulfate corrosion products has not occurred. In this stage, higher sulfate concentrations in the solution result in lower chloride ion content, significantly inhibiting the transmission of chloride ions. Compared to a single salt solution, the chloride ion concentration in a composite solution is lower on the surface and inside due to sulfate inhibition. However, as corrosion progresses, the influence of sulfate on chloride ion transmission changes, marking the beginning of the second stage (after corrosion cracking). By this point, sulfate corrosion has caused the concrete to crack. The cracks control the diffusion coefficient, substantially enhancing ion diffusion capabilities.

In Fig. 7, the effect of sulfate on chloride ion transmission behavior is evident. At x=10 mm, during the first 300 days, sulfate inhibits the transmission of chloride ions in a composite solution, resulting in a lower concentration compared to a single salt solution. After 300 days, due to concrete cracking, the transmission rate of chloride ions accelerates, leading to a rapid increase in concentration that soon surpasses that in a single salt solution. These theoretical calculations demonstrate that sulfate ions inhibit the transmission of chloride ions during the early stages of corrosion but accelerate their diffusion in the later stages. This finding contrasts with the academic view that "chloride and sulfate inhibit each other during the corrosion process."

4.3 Parametric analysis of the influence of fatigue load

To examine the effect of fatigue load on corrosion, the model considered various loading frequencies and stress levels, followed by parametric analysis. Figs. 8 and 9 compare the corrosion effects under static and fatigue loads. At high stress levels, the acceleration of sulfate ion transmission due to fatigue load becomes particularly noticeable. By the 1800th day, the corrosion and failure depths were 43 mm and 36 mm, respectively under stress-free conditions; with a static load, these depths increased to 59 mm and 45 mm, whereas under fatigue load, they reached 71 mm and 52 mm, respectively. Under identical stress levels, fatigue load accelerates corrosion more effectively than static load.

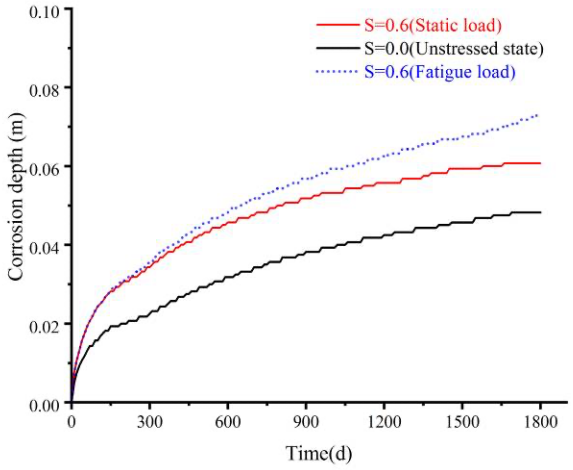

Fig. 8. Corrosion depth curve under fatigue load

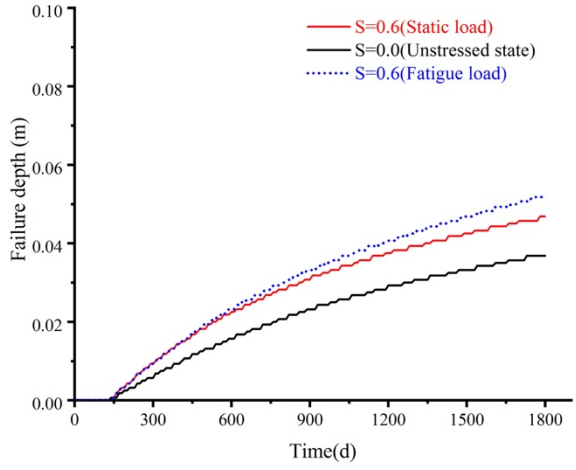

Fig. 9. Failure depth curve under fatigue load

Figs. 10–13 show the effect of loading frequency on corrosion. From Figs. 10 and 11, the accelerated corrosion effect of fatigue load is positively correlated with load frequency at higher stress levels. Corrosion and failure depths increase with the frequency. When the stress level is 0.6 and the load frequency is 12000 times/d, the corrosion

depth exceeds 10 cm by the 1800th day, indicating ion penetration through the specimen. This occurs because fatigue damage increases with the fatigue time, and the corrosion rate is positively related to the level of damage.

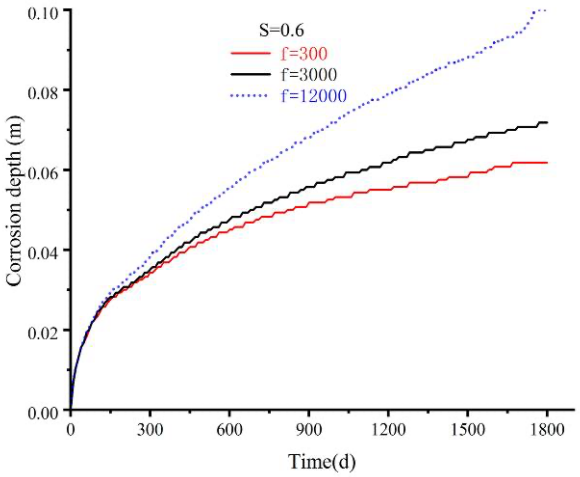

Fig. 10. Effect of loading frequency on corrosion depth (S=0.6)

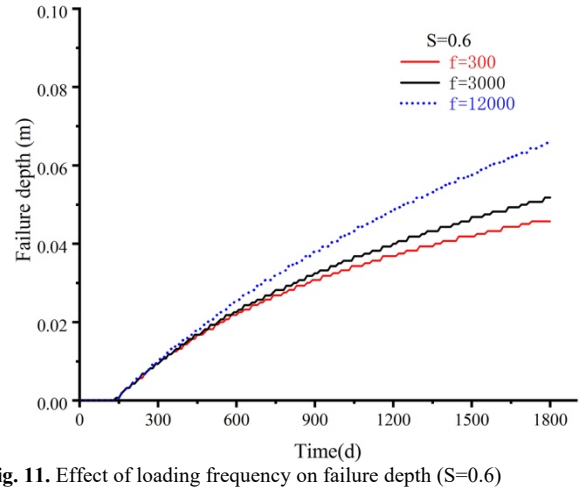

Fig. 11. Effect of loading frequency on failure depth (S=0.6)

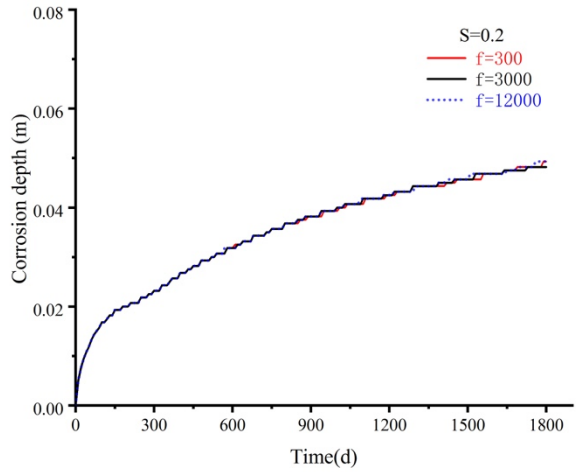

Fig. 12. Effect of loading frequency on corrosion depth (S=0.2)

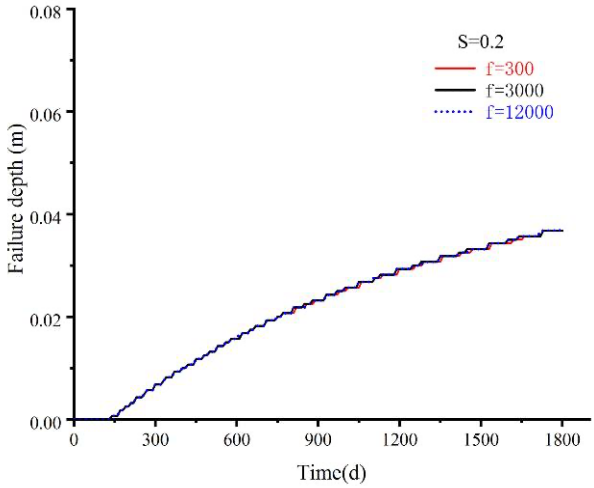

Fig. 13. Effect of loading frequency on failure depth (S=0.2)

Conversely, at low stress levels, the frequency effect is less apparent (Figs. 12 and 13). At a stress level of 0.2, the curves for 300, 3000, and 12000 times/d show minimal differences. According to fatigue theory, the reason is the negligible fatigue damage at low stress levels, rendering the variation in ion transmission capacity due to damage insignificant.

5. Conclusions

To investigate the influence of fatigue load on the corrosion ion transmission process and reveal the coupling relationship between corrosion ion transmission capacity and fatigue parameters, this study established and solved a set of unsteady-state diffusion equations for corrosion ions under fatigue load using mathematical and mechanical analysis methods. The evolution curves for corrosion depth and failure depth under varying stress levels and loading frequencies were presented. Finally, the following conclusions could be drawn:

(1) Chloride ions inhibit the diffusion of sulfate ions throughout the corrosion period. Conversely, sulfate ions have a varying effect on chloride ion transmission: they inhibit chloride ion transmission during the early stages of corrosion but accelerate its diffusion in later stages.

(2) Under high stress levels, fatigue load significantly affects the corrosion ion transmission capacity, with the corrosion rate being positively correlated with the loading frequency and the stress level of fatigue load.

(3) When the stress level is below 0.2, the effect of fatigue load on corrosion ion transmission capacity is negligible.

To more accurately assess the transport behavior of corrosion ions in concrete, the proposed method incorporates the accelerated diffusion effects of corrosion ions due to fatigue loads. However, due to the scarcity of experimental data, especially data on the time-varying concentration of corrosive ions on concrete surfaces under fatigue loading, future research will focus on micro–macro testing of concrete structures subjected to the combined effects of fatigue and corrosion. This will involve modifying the model based on experimental data to gain a better understanding of the micro–macro performance evolution of concrete in complex corrosive environments.

Acknowledgements

This work was supported by the Science and Technology Research Program of Chongqing Municipal Education Commission (Grant No. KJQN202404002), the Natural Science Foundation of Chongqing (Grant No. 2024NSCQ-MSX2005), and the Doctoral Research Funding Project of Chongqing Open University (Grant No. 2023BSZZ-003).

References

[1] J. B. Wang, D. T. Niu, H. He, and B. Wang, "Durability degradation of lining shotcrete exposed to compound salt,"(in Chinese) , *China Civ. Eng. J*., vol. 52, no. 9, pp. 79-90, Sept. 2019.

[2] T. Ikumi and I. Segura, "Numerical assessment of external sulfate attack in concrete structures. A review," *Cement Concrete Res*., vol. 121, pp. 91-105, Apr. 2019.

[3] A. Zahedi, L. Saliba, L. F. M. Sanchez, and A. J. Boyd, "Reliability of the Damage Rating Index to Assess Condition of Concrete Affected by External Sulfate Attack," *Mag. Concrete Res*., vol. 75, no. 3, pp. 135-148, Feb. 2023.

[4] Y. Fernando Silva, S. Delvasto, W. Valencia, and G. Araya-Letelier, "Performance of Self-Compacting Concrete with Residue of Masonry and Recycled Aggregate under Sulfate Attack," *J. Mater. Civil Eng*., vol. 36, no. 1, Jan. 2024, Art. no. 4023491.

[5] R. S. Uwanyuze, L. Enright, J. Y. Zhang, and S. Schafföner, "Preparation of concrete specimen for internal sulfate attack analysis using electron backscatter diffraction," *Int. J. Appl. Ceram. Tec*., vol. 19, no. 3, pp. 1195-1207, Jan. 2022.

[6] N. Cefis, C. Tedeschi, and C. Comi, "External sulfate attack in structural concrete made with Portland-limestone cement: an experimental study," *Can. J. Civil Eng*., vol. 48, no. 7, pp. 731-739, Jul. 2021.

[7] H. Tanyildizi, "Microstructure and Mechanical Properties of Polymer- Phosphazene Mortar Exposed to Sulfate Attack," *ACI Mater. J*., vol. 116, no. 4, pp. 201-208, Jul. 2019.

[8] M. Soleimanirad and H. Rahmani, "The Effect of Chloride Ions on the Resistance of Concretes Containing Aerogel Under Sodium Sulfate Attack," *Int. J. Civ. Eng*., vol. 20, no. 5, pp: 501-512, Jul. 2022.

[9] L. X. Nie, J. Y. Xu, and E. L. Bai, "Dynamic stress-strain relationship of concrete subjected to chloride and sulfate attack," *Constr. Build Mater*., vol. 165, pp: 232-240, Mar. 2018.

[10] P. K. Rusati and K. I. Song, "Magnesium chloride and sulfate attacks on gravel-sand-cement-inorganic binder mixture," *Constr. Build Mater*., vol. 187, pp. 565-571, Oct. 2018.

[11] M. A. Islam, A. J. Golrokh, and Y. Lu, "Chemomechanical modeling of sulfate attack–induced damage process in cement-stabilized pavements," *J. Eng. Mech*., vol. 145, no. 1, Jan. 2019, Art. no. 04018117.

[12] X. D. Chen, X. Gu, X. Z. Xia, and X. Li, "A Chemical-Transport-Mechanics Numerical Model for Concrete under Sulfate Attack," *Materials*., vol. 14, no. 24, Dec. 2021, Art. no. 07710.

[13] X. B. Zuo, Z. K. Zheng, X. N. Li, Y. X. Zou, and L. Li, "Mesoscale numerical simulation on the deterioration of cement-based materials under external sulfate attack," *Eng. Fai.l Anal*., vol. 151, Sept. 2023 , Art. no. 107419.

[14] G. J. Yin, X. B. Zuo, X. N. Li, and Y. X. Zou, "An integrated macro-microscopic model for concrete deterioration under external sulfate attack," *Eng. Fract. Mech*., vol. 240, Jan. 2020, Art. no. 107345.

[15] W. Z. He and L. S. Xu, "Study on evolution model for bearing capacity of tunnel linings exposed to composite corrosive environment," (in Chinese), *China Civ. Eng. J*., vol. 57, no. 1, pp. 122-132, Jan. 2024.

[16] B. W. Guan, T. Yang, J. Y. Wu, A. H. Xu , Y. P. Sheng, and H. X. Chen, "Chloride Transport Behavior of Damaged Concrete under Alternating Load," (in Chinese), *J. Build Mater*., vol. 21, no. 2, pp. 304-308, Apr. 2018.

[17] B. W. Guan, S. F. Chen, Y. P. Sheng, Y. C. Qian, and H. P. Li, "Numerical simulation of sulfate ion migration in cement concrete under corrosion fatigue," *Int. J. Pavement Res. Technol.*, vol. 5, no. 3, pp. 169-175, May. 2012.

[18] N. Li, Z. Q. Jin, Y. Yu, and S. J. Ye, "Generation of real mesoscopic model of concrete and numerical simulation of chloride ions transportation,"(in Chinese), *J. Civ. Environ. Eng*., vol. 41, no. 6, pp. 71-79, Dec. 2019.

[19] Z. Chen, L. Y. Wu, B. Yu, C. F. Yi, and Q. G. Feng, "Coupling model for transport of chloride ion-sulfate ion in concrete subjected to marine environment,"(in Chinese), *Concrete.*, vol. 2018, no. 12, pp. 1-4, Dec. 2018.

[20] L. Jin and X. L. Du, "Variation of porosity and its effect on the deformation process of concrete," (in Chinese), *Eng. Mech*., vol. 30, no. 6, pp. 183-190, Jun. 2013.

[21] T. Ikumi, S. H. P. Cavalaro, I. Segura, and A. Aguado, "Alternative methodology to consider damage and expansions in external sulfate attack modeling," *Cement Concrete Res.*, vol. 63, pp. 105-116, Sept. 2014.